Spatial resolution of synchrotron X-ray microtomography in high energy range: Effect of X-ray energy and sample-to-detector distance

Seo, D.
Department of Mechanical Engineering, Toyohashi University of Technology

Tomizato, F.
Department of Mechanical Engineering, Toyohashi University of Technology

Toda, Hiroyuki
1Department of Mechanical Engineering, Toyohashi University of Technology, Toyohashi

Uesugi, kentaro
Japan Synchrotron Radiation Research Institute

他

https://hdl.handle.net/2324/1807805

出版情報：Applied physics letters. 101 (26), pp.1-, 2012-12-01. American Institute of Physics
バージョン：
権利関係：

Spatial resolution of synchrotron X-ray microtomography in high energy range: Effect of X-ray energy and sample-to-detector distance

D. Seo,[1,a)] F. Tomizato,[1] H. Toda,[1] K. Uesugi,[2] A. Takeuchi,[2] Y. Suzuki,[2] M. Kobayashi[1]

[1]Department of Mechanical Engineering, Toyohashi University of Technology, Toyohashi, Aichi 441-8580, Japan

[2]Japan Synchrotron Radiation Research Institute, Mikazuki, Sayo, Hyogo 679-5198, Japan

[a)]Corresponding author. Tel.: +81 532 44 6695; fax: +81 532 44 6690; E-mail address: seodw@me.tut.ac.jp (D. Seo).

Abstract

Spatial resolution of 3D images obtained by synchrotron X-ray microtomography technique is evaluated using cyclic bar patterns machined on a steel wire. Influences of X-ray energy and the sample-to-detector distance on spatial resolution were investigated. Relatively high X-ray energies of 33-78 keV are applied due to the low X-ray transmission of transition metals. Best spatial resolution of about 1.2 µm was observed at the sample-to-detector distance range of 20-110 mm and at the energy range of 68-78 keV. Several factors such as X-ray scattering and diffraction phenomena affecting the degradation of spatial resolution are also discussed.

Over the past decade, synchrotron X-ray microtomography (XMT) has been performed on light metals such as aluminum with high spatial resolution close to the theoretical limit of the projection-type set-up (about 1 µm).[1-3] However, only a few attempts have been made in the past to apply hard XMT to the transition elements such as ferrous metals due to their low X-ray transmission, even though the necessity of their 3D observations has been recognized. Probability of the photoelectric absorption per unit mass of materials is approximately proportional to Z^3/E^3, where Z is the atomic number of the material and E is the energy of the incident photon.[4] Photoelectric absorption increases with increasing atomic number and decreasing photon energy. This can lead to degradation of contrast and spatial resolution due to poor photon statistics.[3] Such technological limitation in practical application of XMT to transition metals restricts utilizing advanced applications of XMT such as measurements of 3D/4D crack-tip strain fields,[5] local crack driving forces,[6] and spatial distribution of chemical concentrations,[7] which have been developed mainly for light metals. To solve this problem, therefore, the high energy X-ray is essential to acquire the transmitted images of the transition metals.

Several attempts to the transition metals have been made using the high energy beam source. Everette et al.[8] utilized white X-rays to observe elongated voids in HY-100 steel with a spatial resolution of 3 µm at X27A of NSLS. Lame et al.[9] obtained a spatial resolution of 2.7 µm for sintered steel powders using white beam of 35-65 keV with a sample-to-detector (STD) distance of 200 cm at ID15 of ESRF. Narrow fatigue crack of about 10 µm gap (300 µm long) in SUS630 was observed using 35 keV bending beam with a STD distance of 160 mm at BL19B2 of SPring-8.[10] Cheong et al.[11] (90 keV X-ray was used for field of view of 4.34 mm) and Shobu et al.[12] (66.4 keV X-ray was used for field of view of 5.97 mm) used monochromatic X-rays to observe the creep voids or cracks in steels. Although no measurement or no description of spatial resolution is presented in their papers, the spatial resolutions of 19 and 35 μm, respectively, are expected at best, according to the descriptions of sample size and the number of projections. There are wide variations in visible resolution together with applied X-ray energies and STD distances.

Despite its necessity, there are no systematic investigations into the up-to-date spatial resolutions of XMT, especially concerning influence of the applied X-ray energy and the STD distance. It would therefore be of significant value to attain the best achievable spatial resolution level for the transition metals. In this study, the spatial resolution is evaluated by synchrotron XMT technique, as a further study subsequent to author's preliminary research[13] in which only limited STD distances (50-200 mm) at three X-ray energies were considered. The best 3D spatial resolution achievable for high X-ray energies is discussed with the two experimental parameters with more wide ranges, i.e., influence of X-ray energy and STD distance on spatial resolution is evaluated.

XMT was conducted at the undulator beamline BL20XU of SPring-8, Japan. A monochromatic X-ray beam which is produced by a liquid nitrogen-cooled Si (511)-(333) double crystal monochromator was applied with a beam source-to-sample distance of 80 m. When 40 keV energy was used, therefore, the flux density of beam was about 4×10^{11} photons mm^{-2} s^{-1} at sample position.[14] A cooled 2D-CCD image sensor (C4880-41S, Hamamatsu Photonics) of 4000×2624 pixels (pixel size of 5.9 μm×5.9 μm) was used in 2×2 binning mode for acquiring transmitted X-ray images through a 10 μm thick scintillator of Lu_2SiO_5:Ce (LSO) and an ×20 objective. The field of view of the detector was 1000 μm×656 μm. 1500 radiographs were recorded for one scan by scanning 180º with 0.12º step. Isotropic voxels with 0.5 μm edges were obtained in the tomographic volumes reconstructed from 2D projectional radiographs via the filtered back projection algorithm.

In order to examine the effects of experimental parameters on the spatial resolution in all the three directions, the spatial resolution was evaluated using cyclic bar patterns which were machined on a SUS304 stainless steel wire of about 500 μm in diameter (transmission ratio I/I_0 is about 25% at 40 keV) using focused ion beam. The patterns consisted of cyclic gratings with increasing line pitch between 0.51-5.95 μm (0.17-1.96 lp/μm) in the vertical direction and 0.48-5.89 μm (0.17-2.08 lp/μm) in the circumferential direction of cylindrical coordinates, as shown in Fig. 1. Visibility of resolved patterns in the vertical and the circumferential directions was evaluated by the subjective inspection, which was based on reasonable agreement with 5% modulation transfer function (MTF) contrast. For the resolution in the radial direction, the MTF which was derived from an edge response function (ERF) at the outer contour of the wire (i.e., the metal/air interface) was calculated with a threshold of 5% contrast ratio. The eleven different X-ray energies from 33 to 78 keV (with an interval of 5 keV) were used with varying the STD distance from 2 to 140 mm (nine conditions with an interval of 15 mm) to study influence of X-ray energy and the STD distance on spatial resolution.

Fig. 2 shows the virtual cross-sections of 2.21 (in vertical direction; Figs. 2(a) and 2(d)) and 2.65 μm (in circumferential direction; Figs. 2(b) and 2(e)) pitch patterns resolved in the three principal directions with applied beam energy of 40 keV. The upper (Figs. 2(a), 2(b) and 2(c)) and lower slices (Figs. 2(d), 2(e) and 2(f)) were obtained at the STD distance of 20 and 110 mm, respectively. Narrow gratings were clearly resolved at the STD distance of 110 mm, as shown in Figs. 2(d) (2.21 μm pitch) and 2(e) (2.65 μm pitch). In contrast, however, it was difficult to recognize the cyclic patterns acquired at the distance of 20 mm because of the extreme blurring in both directions, as shown in Figs. 2(a) and 2(b).

At the radial direction (Figs. 2(c) and 2(f)), a strong blur of the steel/air interface was also observed as a dark and bright fringe gap between overshoot and undershoot of gray values, leading to a loss of image contrast. The blurring is caused by fringe generation at the interface edge which is due to photon diffraction.[15] The fringe width β is proportional to $(\lambda L)^{1/2}$, where λ is wavelength at corresponding photon energy (e.g., λ = 0.31 angstrom at 40 keV) and L is the STD distance.[16,17] The width of fringe increases with increase of the STD distance (e.g., β = 1.84 μm at L=110 mm, while β = 0.78 μm at L=20 mm). Therefore, this diffraction constraint could be improved by controlling the STD distance. If the STD distance becomes short, however, the spatial resolution will be also affected by a forward scattering phenomenon as one of negative effects on the resolution.[4]

At 40 and 73 keV, the variations of spatial resolution in the vertical, the circumferential and the radial directions according to the STD distance are shown in Figs. 3(a), 3(b) and 3(c), respectively. The vertical resolution was enhanced up to about 1.2 μm in the distance range of 20-110 mm at both 40 and 73 keV, as shown in Fig. 3(a). The circumferential resolution in the distance range of 35-140 mm was also enhanced up to about 1.8 μm at both 40 and 73 keV, as shown in Fig. 3(b). The enhancement of the radial resolution at both 40 and 73 keV, however, was started from the relatively long distance of 65 mm shown in Fig. 3(c), and reached up to about 1.6 µm. Although all the best resolutions in the three directions were observed at 73 keV, the spatial resolutions at the energy of 40 keV, in the case of the vertical (over L=20 mm) and the circumferential (over L=35 mm) directions, were almost similar with them at 73 keV with a negligible difference. In the case of STD distance of 110 mm, for example, the vertical spatial resolution at 40 keV was 1.46 µm, while 1.28 µm at 73 keV. It was confirmed that the vertical resolution exceeds the circumferential and radial resolution at both 40 and 73 keV.

The closer the samples were to the detector, however, the more the spatial resolutions were degraded in all directions due to the forward scattering as mentioned above. The sharp deteriorations were observed in the short range of STD; i.e., 35 and 65 mm at circumferential and radial directions, respectively. In the case of vertical direction, the drop in spatial resolution started from more short distance of 20 mm, as shown in Fig. 3(a). This effect was amplified at higher energy of 73 keV.

A series of these deteriorations could be explained by Compton scattering theory.[4] A scattered photon which is received the partial energy of incident X-ray travels out of the trajectory of the incident photon after Compton scatter interaction, i.e., it scatters through any angle from 0° to 180° relative to incident photon angle with a reduced frequency and therefore reduced energy. Compton scattered x-rays can deleteriously affect image quality by reducing contrast. From Klein-Nishina formula, the energy of the scattered photon E_S relative to the incident photon E_0 for a photon scattering angle θ is given as follows:[4,18]

$$\frac{E_S}{E_0} = \frac{1}{1+\frac{E_0}{511\,keV}(1-\cos\theta)} \quad (1),$$

where 511 keV is the energy equal to the rest mass of the electron. From above, the θ becomes wider as the E_S decreases. At higher energies, the photon scattering is weighted in relatively smaller angle region (e.g., 30-60° at 80 keV) comparing to the low-level energies such as 20 keV.[4] In the case of STD distance of 2 mm, for example, the photons scattered up to about 14° (at the object surface) can be penetrated to the LSO scintillator and then affect the projection images of effective object size of 500 µm.

From Fig. 3, the spatial resolution measured at 73 keV exhibit the superior results in the STD distance of over 50 mm. This may be associated with the characteristics of the lutetium-based scintillator employed in this study. The volume of the scintillator in which X-rays are absorbed and the scintillation photons are produced is generally dependent on the X-ray energy. The absorption mean free path of X-ray radiation also depends on photon energy at high X-ray energies. This is because the spreading of the visible photons produced in the scintillator acts to blur the image. It is notable that lutetium used as a scintillator has K absorption edge at 63.31 keV and this inevitably causes the smallest absorption mean free path at 73 keV compared to 40 keV, thereby resulting in beneficial effects on the spatial resolution.[13]

The variations of spatial resolutions according to the X-ray energies in vertical, circumferential and radial directions are shown in Figs. 4(a), 4(b) and 4(c), respectively. The STD distance was fixed at 110 mm which provides the best spatial resolution in all the three directions, as shown in Fig. 3. The visible resolutions observed in each direction were increased up to about 1.2 µm (at 68-78 keV in vertical direction), 1.8 µm (at 73-78 keV in circumferential direction) and 1.6 µm (at 73-78 keV in radial direction), respectively. The resolutions in all directions started to be enhanced from around 70 keV because of becoming shorter in the mean free path of lutetium, as discussed previously.

Difference in the spatial resolution between vertical and circumferential resolutions was observed in Figs. 3 and 4 because of different size of incident beam in vertical and horizontal directions. The beam size in the horizontal direction can be controlled by a font-end slit installed at a distance of 31 m from the light source. The spatial coherence can be defined by the width of this slit which was 0.4 mm in this study. If the STD distance is 110 mm, the penumbral blur (equivalent to the full width at half maximum) becomes the resolution of 1 µm which cannot be neglected. In contrast, the beam size in vertical direction was 15 µm which was much smaller than the horizontal size. Therefore, the effect of penumbral blurring was negligible. In practical use, the vertical beam is degraded because of vibration of the monochromator crystal. The effective beam size, therefore, will be about 40 µm. On balance, the vertical resolution of the penumbral blur based on geometrical optics consideration was 0.05 µm at STD distance of 110 mm and can be treated as of negligible value.

The deflection of X-ray beam which was constant and integrated in vertical direction could be regarded as one of positive effects on the superior vertical resolution, because the vertical gratings on the test object were always parallel to the beam. Oversampling effect could be also considered as another positive effect, i.e., the sampling pitch becomes finer vertically due to the vertical wobbling of test object.

As a practical application, a 6 μm-long inclusion in a stainless steel (Fig. 5(a)) was observed by XMT though a typical 3D rendering process. The raw radiograph data obtained by X-ray scanning was reconstructed to a 3D volume data set using the filtered back-projection algorithm. The slice images (Fig. 5(b)) were, then, stacked and rendered to produce 3D images (Fig. 5(d)) with an isotropic voxel size of about 0.5 μm3 using a commercial visualization software. Segmentation technique was performed to extract a different component from the matrix using the different gray values between voxels which is based on the different X-ray absorption between dissimilar materials. Fig. 5(c) shows a line profile of gray value across an inclusion-matrix interface. Since the inclusion has an incoherent interface with the stainless steel matrix, a sharp discontinuity in the linear absorption coefficient (i.e., gray value) was observed at its edge. It is obvious that a high resolution system produces such a sharp image with a steep slope at the edge, whereas a low resolution system will produce a blurred edge image with a gentle slope.

In summary, this study has shown that spatial resolution of cyclic bar patterns machined on a stainless steel wire by using the technique of synchrotron XMT. Especially, influence of the STD distance and X-ray energy on the spatial resolution was emphasized. As the results, considerably high resolution has been achieved, which is close to the theoretical uppermost limit in the projection-type X-ray tomography. Best spatial resolution of about 1.2 µm (at vertical direction) was observed at the STD distance range of 20-110 mm and at the energy range of 68-78 keV. If the STD distance becomes short, the penetration rate of the Compton scattering photons increased and resulted in the deterioration of spatial resolution. Big deterioration of spatial resolution around 63 keV were observed at the STD distance of 110 mm because of the K absorption edge of lutetium scintillator at 63.31 keV.

This work was undertaken as a research project of the ISIJ Innovative Program for Advanced Technology. The synchrotron radiation experiment was performed with the approval of JASRI through proposal numbers 2011A1263 and 2011B1111.

[1]H. Toda, K. Uesugi, A. Takeuchi, K. Minami, M. Kobayashi, and T. Kobayashi, Appl. Phys. Lett. **89**, 143112 (2006).

[2]H. Toda, T. Hidaka, M. Kobayashi, K. Uesugi, A. Takeuchi, and K. Horikawa, Acta Mater. **57**, 2277 (2009).

[3]R. Mizutani, A. Takeuchi, R. Y. Osamura, S. Takekoshi, K. Uesugi, and Y. Suzuki, Micron **41**, 90 (2010).

[4]J. A. Seibert and J. M. Boone, J. Nucl. Med. Technol. **33**, 3 (2005).

[5]L. Qian, H. Toda, K. Uesugi, M. Kobayashi, and T. Kobayashi, Phys. Rev. Lett. **100**, 115505 (2008).

[6]H. Toda, S. Yamamoto, M. Kobayashi, and K. Uesugi, Acta Mater. 56 (2008) 6027.

[7]H. Toda, T. Nishimura, K. Uesugi, Y. Suzuki, and M. Kobayashi, Acta Mater. **58**, 2014 (2010).

[8] R. K. Everett, K. E. Simmonds, and A. B. Geltmacher, Scrpta Mater. **44**, 165 (2001).

[9] O. Lame, D. Bellet, M. D. Michiel, and D. Bouvard, Acta Mater. **52**, 977 (2004).

[10] D. Shiozawa, Y. Nakai, T. Kurimura, Y. Morikage, H. Tanaka, H. Okado, T. Miyashita, and K. Kajiwara, J. Soc. Mater. Sci. **56**, 951 (2007).

[11] K. S. Cheong, K. J. Stevens, Y. Suzuki, K. Uesugi, and A. Takeuchi, Mater. Sci. Eng. A. **513-514**, 222 (2009).

[12] T. Shobu, K. Tanaka, A. Hashimoto, and J. Narita, J. Soc. Mater. Sci. **58**, 588 (2009).

[13] H. Toda, F. Tomizato, F. Zeismann, Y. Motoyashiki-Besel, K. Uesugi, A. Takeuchi, Y. Suzuki, M. Kobayashi, and A. Brueckner-Foit, ISIJ Int. **52**, 516 (2012).

[14] Y. Suzuki, K. Uesugi, N. Takimoto, T. Fukui, K. Aoyama, A. Takeuchi, H. Takano, N. Yagi, T. Mochizuki, S. Goto, K. Takeshita, S. Takahashi, H. Ohashi, Y. Furukawa, T. Ohata, T. Matsushita, Y. Ishizawa, H. Yamazaki, M. Yabashi, T. Tanaka, H. Kitamura, and T. Ishikawa, AIP Conf. Proc. **705**, 344 (2004).

[15] M. Stampanoni, G. Borchert, P. Wyss, R. Abela, B. Patterson, S. Hunt, D. Vermeulen, and P. Ruegsegger, Nucl. Instrum. Meth. A **491**, 291 (2002).

[16] P. Cloetens, M. Pateyron-Salome, J. Y. Buffiere, G. Peix, J. Baruchel, F. Peyrin, and M. Schlenker, J. Appl. Phys. **81**, 5878 (1997).

[17] T. Hidaka, H. Toda, M. Kobayashi, K. Uesugi, and T. Kobayashi, J. Jpn. Inst. Light Met. **58**, 58 (2008).

[18] O. Klein and Y. Nishina, Z. Phys. **52**, 853 (1929).

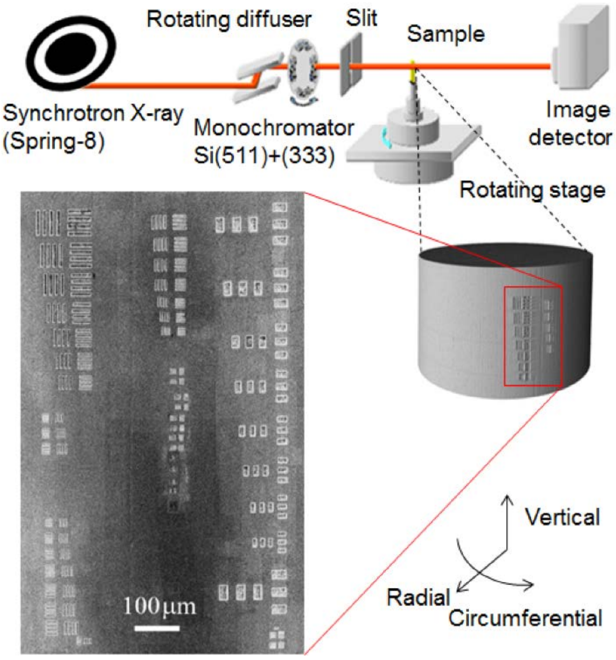

FIG. 1. Cyclic bar patterns machined on a stainless steel wire of about 500 µm in diameter.

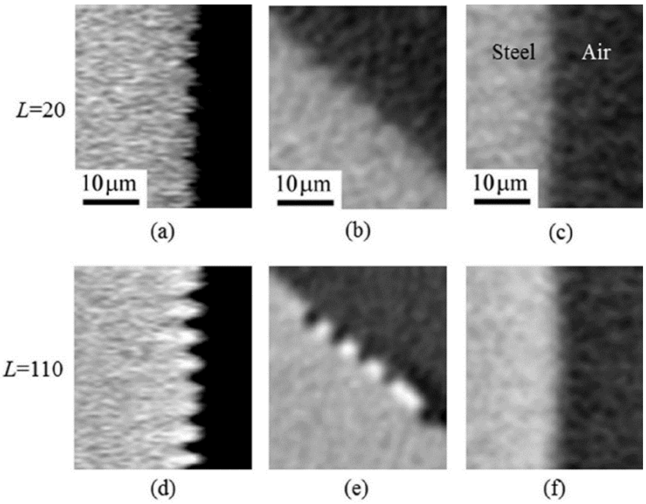

FIG. 2. Virtual cross-sections captured at 40 keV and two STD distance of 20 and 110 mm; (a) and (d) in vertical direction; (b) and (e) in circumferential direction; (c) and (f) in radial direction.

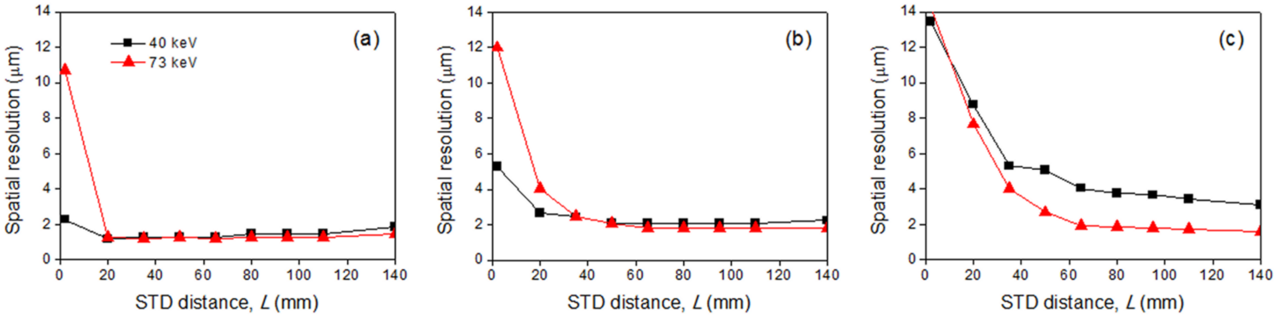

FIG. 3. Variations in spatial resolution as a function of STD distance in (a) vertical, (b) circumferential and (c) radial directions.

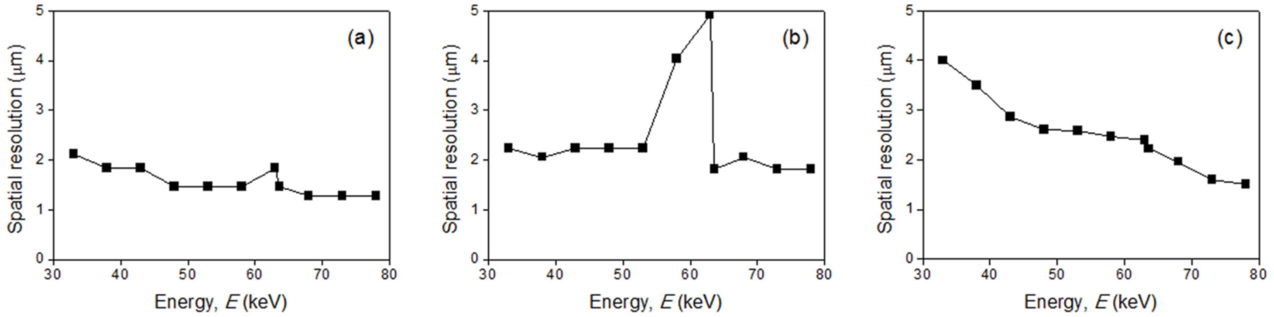

FIG. 4. Variations in spatial resolution at STD distance of 110 mm as a function of X-ray energy in (a) vertical, (b) circumferential and (c) radial directions.

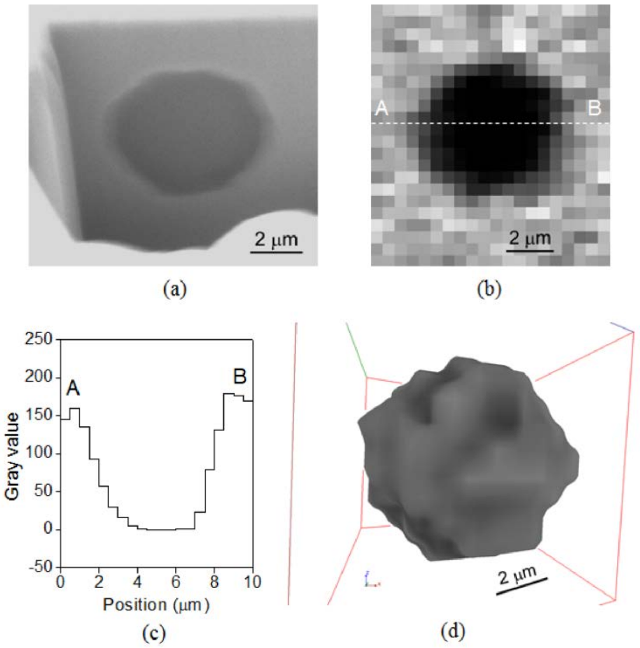

FIG. 5. (a) Cross-sectional view of an inclusion machined by FIB, (b) a virtual tomographic slice of section (a), (c) gray values across line AB in (b), and (d) a reconstructed 3D volume image.